

A theoretical model for quantifying the imprinting sensitivity of direct-drive inertial confinement fusion implosions

Dongxue Liu,¹ Jiaqin Dong,^{1,*} Yunxing Liu,¹ Zhiyu He,¹ Wei

Wang,¹ Yuqiu Gu,¹ Xiuguang Huang,¹ and Jian Zheng^{2,3}

¹*Shanghai Institute of Laser Plasma, Shanghai 201800, China*

²*Department of Plasma Physics and Fusion Engineering,
and CAS Key Laboratory of Frontier Physics in Controlled Nuclear Fusion,
University of Science and Technology of China,
Hefei 230026, People's Republic of China*

³*Collaborative Innovation Center of IFSA, Shanghai Jiao Tong University,
Shanghai, 200240, People's Republic of China*

(Dated: March 3, 2026)

Abstract

To quantify the sensitivity of diverse implosion designs to laser imprinting, we developed an equivalent perturbation model that maps laser imprinting as the target surface perturbation. By incorporating imperfections in target fabrication and thermal smoothing in the plasma, the model shows a reduced implosion sensitivity to laser imprinting, extending the analysis beyond geometric irradiation. The imprinting sensitivity threshold is defined as $\frac{\delta h_{\text{las}}}{\delta h_{\text{tar}}} = 0.1$. When the imprinting amplitude δh_{las} is less than one-tenth of the target perturbation amplitude δh_{tar} , target perturbations dominate. Radiation-hydrodynamics simulations confirm that when $\frac{\delta h_{\text{las}}}{\delta h_{\text{tar}}} \leq 0.1$, variations in nonlinear onset time and adiabat remain within 12% of those observed with target perturbations alone. Moreover, the imprinting sensitivity is supported by OMEGA experiments. These results indicate that joint control of laser and target perturbations, improving target quality when $\frac{\delta h_{\text{las}}}{\delta h_{\text{tar}}} \leq 0.1$ and laser smoothing otherwise, can support stable implosions for high-gain direct-drive inertial confinement fusion.

Keywords: implosion sensitivity, laser imprinting, equivalent perturbation model, direct-drive inertial confinement fusion

PACS numbers:

*e-mail:dongjiaqin@hotmail.com

I. INTRODUCTION

The achievement of ignition [1–3] at the National Ignition Facility (NIF) marks a historic milestone in inertial confinement fusion (ICF). However, the intermediate conversion of laser energy to X-rays in these indirect-drive experiments limits high-gain ignition. Direct-drive ICF [4] represents a more efficient laser–target coupling path to high gain, but faces significant challenges early in the implosion. The conduction zone between the critical density surface and the ablation front is insufficient to smooth out spatial nonuniformity in the deposited laser energy [5]. Consequently, spatial variations in laser intensity [6–8] and inherent target imperfections [9] can trigger the Richtmyer–Meshkov (RM) [10, 11] instability and seed the Rayleigh–Taylor (RT) instability at the ablation front. Once amplified by RT growth, these perturbations lead to an experimentally observable degradation, i.e., shell deformation and shell thickening due to adiabat elevation [12].

A detailed study of RT is essential to assess implosion performance and develop mitigation strategies. Single-mode RT perturbations grow exponentially [13–15] before the low-density bubble region expands linearly in the nonlinear regime [16]. Multimode RT perturbations transition from exponential to quadratic growth [17–19]. Consequently, strategies, such as pulse shaping [20, 21], doped targets [22, 23], and foam coated targets [24], have been proposed to reduce the linear growth rate to delay the nonlinear transition. However, suppressing RT linear growth rate alone does not guarantee a stable implosion [25] due to the seeding of multiple perturbations.

Substantial research has been devoted to understanding and mitigating the seeding of perturbations. Various target imperfections [10, 26–30], which are pre-existing, grow and undergo damped oscillations via the ablative RM. In contrast, laser imprinting continues until $kD_{ac} > 1$ and may undergo damped oscillations [7, 31, 32], where k is the perturbed wavenumber and D_{ac} represents the width of the conduction zone. To mitigate imprinting, beam-smoothing techniques such as phase plates (PP) [33, 34], smoothing by spectral dispersion (SSD) [35, 36], and polarization smoothing (PS) [37, 38] have been developed. In SSD-smoothed, kilojoule-class experiments on OMEGA [39], the performance of high-adiabat implosions saturates even when the root-mean-square (rms) of laser deposition remains above the 1%, a sensitivity threshold reported by Skupsky et al [35]. This implies that target imperfections and plasma smoothing can reduce the imprinting sensitivity, thus motivating a general model to quantify the imprinting sensitivity in diverse implosion designs.

In the paper, we developed an equivalent perturbation model that treats laser imprinting as

target surface perturbation. The model reveals that the shift in the nonlinear onset time due to laser imprinting, when plotted against $\frac{\delta h_{\text{tar}}}{\delta h_{\text{las}}}$, exhibits a slope transition. This transition defines the imprinting sensitivity threshold as $\frac{\delta h_{\text{tar}}}{\delta h_{\text{las}}} = 0.1$. Radiation-hydrodynamics simulations validate that when $\frac{\delta h_{\text{las}}}{\delta h_{\text{tar}}} \leq 0.1$, the variation in the nonlinear onset time and adiabat at the start of the acceleration phase remains within 12%, compared to simulations with only target perturbations. Moreover, the imprinting sensitivity is also supported by OMEGA experiments. These results indicate that joint control of laser and target perturbations, improving target quality when $\frac{\delta h_{\text{tar}}}{\delta h_{\text{las}}} \leq 0.1$ and laser smoothing otherwise, can support stable implosions for high-gain direct-drive inertial confinement fusion.

The paper is organized as follows. In Section II, an equivalent perturbation model is developed to quantify laser imprinting amplitude δh_{las} and imprinting sensitivity in various implosion designs. In Section III, the model is validated using radiation-hydrodynamic simulations. The imprinting sensitivity is also supported by OMEGA experiments and it suggests joint control of laser and target perturbations. In Section IV, we draw our conclusions.

II. EQUIVALENT PERTURBATION MODEL

In direct-drive ICF, laser nonuniformity is characterized by a dimensionless relative intensity variation, whereas target surface roughness is quantified in units of μm . Therefore, based on the different seeding process, we developed an equivalent-perturbation model that maps laser imprinting as the corresponding target perturbation at the outer surface. By incorporating target perturbations and plasma smoothing, the model quantifies the implosion sensitivity to laser imprinting, extending the analysis beyond geometric irradiation.

A. Perturbation seeding process

To clarify the distinctions between different seeding processes, we neglect the RM instability, i.e., oscillations arising from both dynamic overpressure and the convection of shock-induced vorticity, as well as growth resulting from the perturbed field [7]. This simplification is justified because the evolution of the RM instability is alike for equivalent target perturbations and laser imprinting.

Figs. 1(a, b) illuminate the seeding of laser nonuniformity (δ_{las}) and target surface perturbation

(δ_{tar}). As shown in Fig. 1(b), the higher laser energy deposition increases the mass ablation rate, which in turn causes a local depression of the target. Consequently, when laser nonuniformity δ_{las} is in phase with target surface perturbation δ_{tar} , laser imprinting (δh_{las}) becomes antiphase (i.e., a phase difference of π) with inherent target perturbations (δh_{tar}).

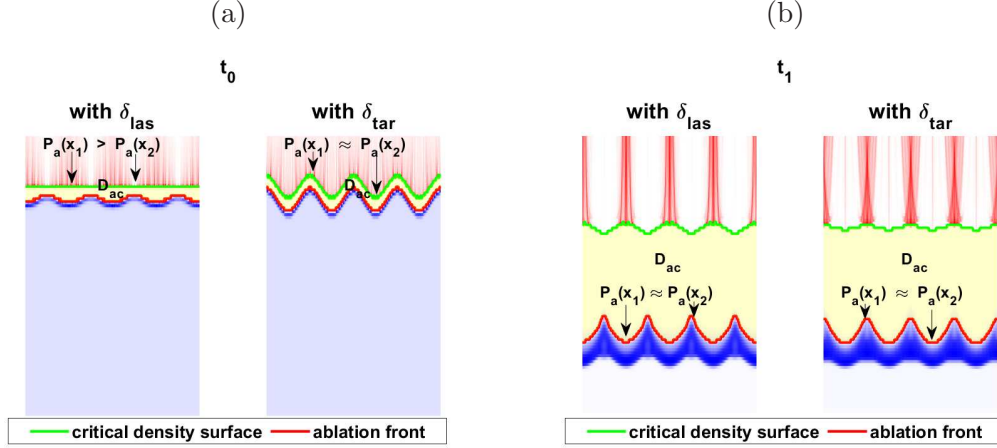


FIG. 1: Illustration of the seeding process for δ_{las} and δ_{tar} (a) Early in irradiation, the conduction zone, denoted by the yellow shaded area, is too short to smooth the laser-imprinted pressure perturbation $\delta P_a = P_a(x_1) - P_a(x_2)$. In contrast, the ablative pressure P_a is nearly uniform at the ablation front perturbed by δ_{tar} , except for slight modulations caused by ray deflection. (b) Later, the extended conduction zone smooths δP_a caused by δ_{las} and ray deflection toward high-density regions. In both panels, the blue and red shades represent normalized target density and laser energy deposition, respectively, with lower opacity corresponding to lower values. Detailed simulation setup can be found in the Appendix.

For laser nonuniformity (δ_{las}), the short conduction zone D_{ac} cannot smooth the laser deposition variations in Fig. 1(a). This modulates ablative pressure, producing fluctuations in ablative velocity that deform the ablation front in Fig. 1(b). Thus, laser imprinting depends not only on δ_{las} , but also on the ablative history. In contrast, for target perturbations (δ_{tar}), the ablative pressure remains nearly uniform on the perturbed ablation front. This is because the energy deposition is initially uniform in Fig. 1(a), and later perturbed energy deposition caused by ray deflection is smoothed by the extended conduction zone in Fig. 1(b). Thus, the deformation of the ablation front can be traced directly to δ_{tar} .

B. Model derivation

Building on the seeding process, we developed an equivalent perturbation model for laser perturbations that satisfy $kD_{ac}(t) \leq 1$ early in irradiation. The model relates the imprinted laser nonuniformity to the equivalent target perturbation at the outer surface.

Following the cloudy-day model [5], pressure nonuniformity with wavenumber k decays exponentially as $e^{-kD_{ac}(t)}$. Under steady ablation of polyethylene, the ablative pressure and velocity are given by [40]:

$$P_a = 11.9 (I_L/\lambda_L)^{2/3} \quad [\text{Mbar}], \quad (1)$$

$$v_a = 3.08 \times 10^5 (I_L/\lambda_L^4)^{1/3} / \rho_a \quad [\text{cm/s}], \quad (2)$$

where the laser power I_L is in $10^{14}\text{W}/\text{cm}^2$, the density on the ablation front ρ_a is in g/cm^3 , and the laser wavelength λ_L is in μm . The corresponding nonuniformity in ablative velocity decays as $e^{-kD_{ac}(t)/2}$, yielding:

$$\begin{aligned} \delta v_{a+}(t) &= v_a \left(\left(1 + \frac{\delta I_L}{I_L} \right)^{1/3} - 1^{1/3} \right) e^{-kD_{ac}(t)/2} \quad [\text{cm/s}], \\ \delta v_{a-}(t) &= v_a \left(1^{1/3} - \left(1 - \frac{\delta I_L}{I_L} \right)^{1/3} \right) e^{-kD_{ac}(t)/2} \quad [\text{cm/s}], \end{aligned} \quad (3)$$

where $\delta v_{a+}(t)$ and $\delta v_{a-}(t)$ are the maximum and minimum perturbations in ablative velocity. The linear deformation of the ablation front is obtained by integrating $\delta v_a(t)$ over the period during which the conduction zone remains insufficient to smooth the laser imprinting, i.e. $kD_{ac}(t) \leq 1$:

$$\delta h_{\text{las}} = \frac{1}{2} \left(\int_{kD_{ac}(t) \leq 1} \delta v_{a+}(t) dt + \int_{kD_{ac}(t) \leq 1} \delta v_{a-}(t) dt \right) \quad [\text{cm}]. \quad (4)$$

Here, $\frac{\delta h_{\text{las}}}{\delta h_{\text{tar}}} = 1$ at $kD_{ac} = 1$ implies that the laser imprinting amplitude is equivalent to the target surface perturbation amplitude. This equivalence is not a simple linear function of δ_{las} ; it depends critically on the laser pulse and the perturbed wavelength through δv_a .

C. Quantifying imprinting sensitivity

OMEGA experiments demonstrate that target perturbations and plasma smoothing can reduce the implosion sensitivity to laser imprinting [39]. Using the equivalent perturbation model, we quantify $\frac{\delta h_{\text{las}}}{\delta h_{\text{tar}}}$ that incorporates the effects of both target perturbations and plasma smoothing, and we derive the resulting shift in nonlinear onset time due to laser imprinting. The dependence

of the shift on $\frac{\delta h_{\text{las}}}{\delta h_{\text{tar}}}$ determines the imprinting sensitivity. When the implosion is insensitive to laser imprinting, it resides in a target-dominant regime governed by target perturbations.

We analyze how the coexistence of δ_{las} and δ_{tar} affects the nonlinear onset time compared to the scenario with δ_{tar} alone. Following previous work [41], the nonlinear onset time for a single-mode perturbation is defined as when its amplitude reaches 0.1λ . For a reference perturbation with $\delta h_{\text{ref}} = 2 \mu\text{m}$ and $\lambda_{\text{ref}} = 50 \mu\text{m}$ at the onset of acceleration, the reference onset time t_{ref} is:

$$t_{\text{ref}} = \frac{1}{\gamma_{50}} \ln\left(\frac{5}{2}\right), \quad (5)$$

where γ_{50} is the linear growth rate of λ_{ref} . Note that when $kD_{ac} > 1$, the relative intensity of the single-mode laser and target perturbations remains $\delta h_{\text{las}}/\delta h_{\text{tar}}$ due to the same RM growth. Thus, when δ_{las} and δ_{tar} are in phase, laser imprinting (δh_{las}) becomes antiphase (i.e., a phase difference of π) with inherent target perturbations (δh_{tar}), the total perturbed amplitude is reduced, delaying the nonlinear onset time:

$$t_{\text{lt}} - t_t = \frac{-\ln\left(1 - \frac{\delta h_{\text{las}}}{\delta h_{\text{tar}}}\right)}{\ln(5/2)} \frac{\gamma_{50}}{\gamma_\lambda} t_{\text{ref}}. \quad (6)$$

Here, t_{lt} and t_t denote the nonlinear onset time with both perturbations and with only target perturbations, respectively, γ_λ represents the linear growth rate of the single-mode perturbation, and the range of $\frac{\delta h_{\text{las}}}{\delta h_{\text{tar}}}$ is zero to one. Conversely, when δ_{las} and δ_{tar} are antiphase, the nonlinear onset time advances:

$$t_{\text{lt}} - t_t = \frac{-\ln\left(1 + \frac{\delta h_{\text{las}}}{\delta h_{\text{tar}}}\right)}{\ln(5/2)} \frac{\gamma_{50}}{\gamma_\lambda} t_{\text{ref}}. \quad (7)$$

Fig. 2(a) plots Eq. 6 and Eq. 7 for $\gamma_\lambda = \gamma_{50}$. $t_{\text{lt}} - t_t$ approaches zero for the weak laser imprinting amplitude and diverges as $\frac{\delta h_{\text{las}}}{\delta h_{\text{tar}}} \rightarrow 1$. The slope $\mathcal{S} = \frac{d(t_{\text{lt}} - t_t)}{d(\delta h_{\text{las}}/\delta h_{\text{tar}})}$ measures how rapidly the nonlinear onset changes with imprinting. Fig. 2(b) shows \mathcal{S} as a function of $\frac{\delta h_{\text{las}}}{\delta h_{\text{tar}}}$. Its behavior reveals a clear transition: \mathcal{S} increases linearly for $\frac{\delta h_{\text{las}}}{\delta h_{\text{tar}}} \leq 0.1$ but grows nonlinearly thereafter. This transition defines the imprinting sensitivity threshold:

$$\frac{\delta h_{\text{las}}}{\delta h_{\text{tar}}} = 0.1. \quad (8)$$

A target-dominant regime is then characterized by $\frac{\delta h_{\text{las}}}{\delta h_{\text{tar}}} \leq 0.1$. Within this regime, the relative shift in the nonlinear onset time, $(t_{\text{lt}} - t_t)/t_{\text{ref}}$, remains below 12%.

Realistic implosions involve multimode spectra with mixed phase relationships. We characterize the initial perturbation level using the root-mean-square (rms). The nonlinear stage begins when

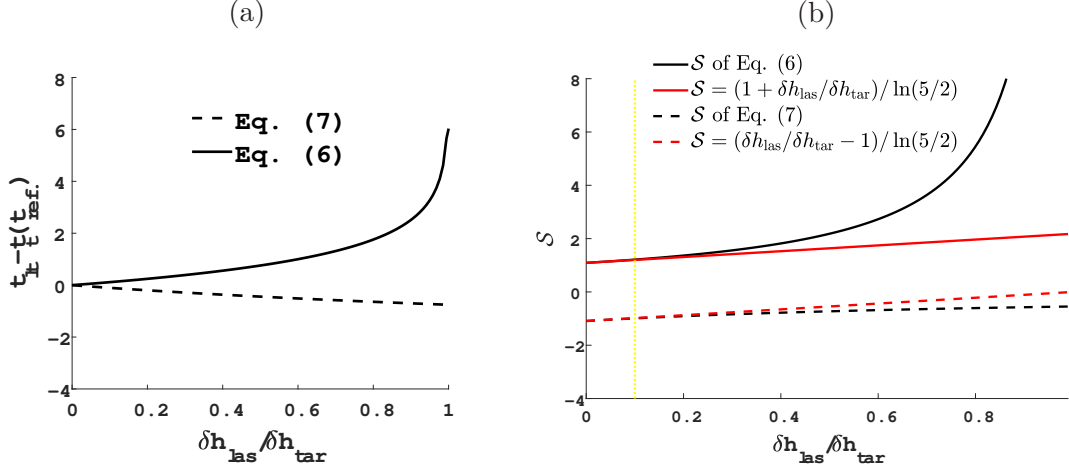


FIG. 2: Evolution of $t_{lt} - t_t$ (a) and $\mathcal{S} = \frac{d(t_{lt} - t_t)}{d(\delta h_{\text{las}} / \delta h_{\text{tar}})}$ (b) as a function of $\frac{\delta h_{\text{las}}}{\delta h_{\text{tar}}}$. In (a), the solid line shows the delay when laser perturbations mitigate target perturbations; the dashed line shows the advancement caused by laser imprinting. In (b), \mathcal{S} shifts from linear to nonlinear growth as increasing $\frac{\delta h_{\text{las}}}{\delta h_{\text{tar}}}$. The onset of this transition, marked by the yellow dotted line, occurs at $\frac{\delta h_{\text{las}}}{\delta h_{\text{tar}}} = 0.1$. The red lines fit the linear growth of \mathcal{S} .

the maximum deformation reaches $0.1\lambda_{\text{ran}}$, where λ_{ran} is the perturbed wavelength range. In the worst scenario, δh_{las} and δh_{tar} are antiphase, and the shift in the nonlinear onset time becomes

$$t_{lt} - t_t = \frac{-\ln\left(1 + \frac{\text{rms}_{\text{las}}}{\text{rms}_{\text{tar}}}\right)}{\ln(5/2)} \frac{\gamma_{50}}{\gamma_{\lambda_{\text{ran}}}} t_{\text{ref}}. \quad (9)$$

The imprinting sensitivity threshold remains similar. For $\frac{\text{rms}_{\text{las}}}{\text{rms}_{\text{tar}}} \leq 0.1$ and $\gamma_{\lambda} = \gamma_{50}$, $\frac{t_{lt} - t_t}{t_{\text{ref}}}$ remains below 12%.

III. MULTIDIMENSIONAL VALIDATION OF THE MODEL

A. Simulation validation of the equivalent perturbation model

We validate the equivalent perturbation model (Eq. 4) by comparing two distinct hydrodynamic scenarios: one involves laser imprinting and the other involves target perturbations. Validation cases 1-16 (see Appendix Table II) were performed using the Eulerian radiation-hydrodynamics code FLASH [42]. Under two different laser pulses, all cases satisfy $\frac{\delta h_{\text{las}}}{\delta h_{\text{tar}}} \approx 1$ at $kD_{\text{ac}} \approx 1$, indicating the model's potential applicability in various implosion designs.

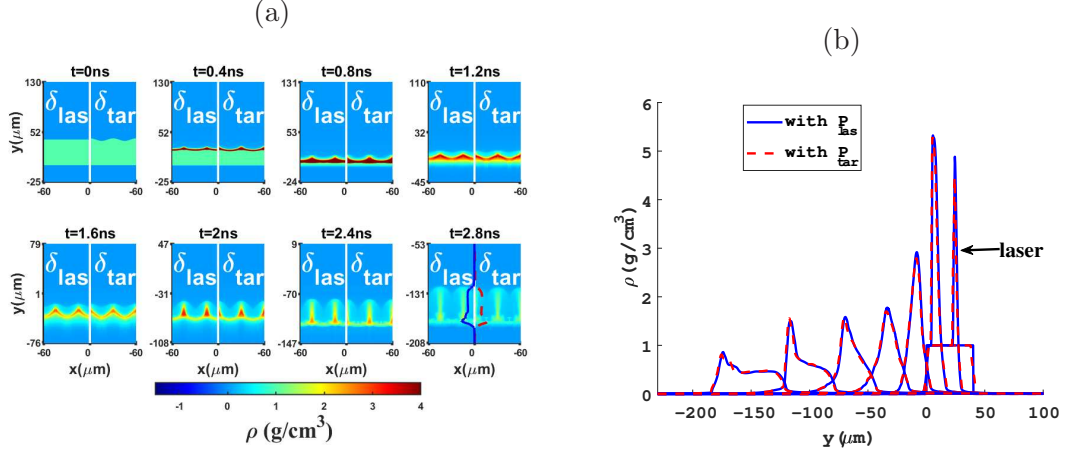


FIG. 3: Temporal evolution of (a) the two-dimensional (2D) and (b) the corresponding vertically averaged one-dimensional (1D) density distribution. In (a), the left region of the white line corresponds to simulations with δ_{las} , while the right region denotes simulations with δ_{tar} . The red and blue lines at $t = 2.8$ ns mark the 1D density profiles in (b). The similar 2D and 1D density distributions indicate that the laser imprinting amplitude δh_{las} equal the inherent target perturbation amplitude δh_{tar} .

The typical simulation results are shown in Fig. 3. In Fig. 3(a), the left region of the white line corresponds to simulations with δ_{las} , while the right region denotes simulations with δ_{tar} . Initially, before $t = 0.8$ ns, the perturbation amplitude on the right is larger than that on the left. This difference decreases over time and eventually vanishes. The corresponding vertically averaged 1D density profiles are shown in Fig. 3(b). As time proceeds from left to right, the spatial width of the compressed shell becomes comparable for both perturbation sources. These consistencies confirm that both the wavelength and amplitude of laser imprinting and inherent target perturbations are similar. Nevertheless, detailed differences in density distributions persist, which can be attributed to differences in the seeding process.

B. Simulation validation for imprinting sensitivity

When the imprinting amplitude is lower than the implosion sensitivity threshold, expressed as Eq. 8, the implosion resides in a target-dominant regime. Radiation-hydrodynamic simulations confirm that within the target-dominant regime, laser imprinting slightly alters the nonlinear onset

time and the adiabat at the start of the acceleration phase. This change is less than 12% compared to simulations containing only δ_{tar} .

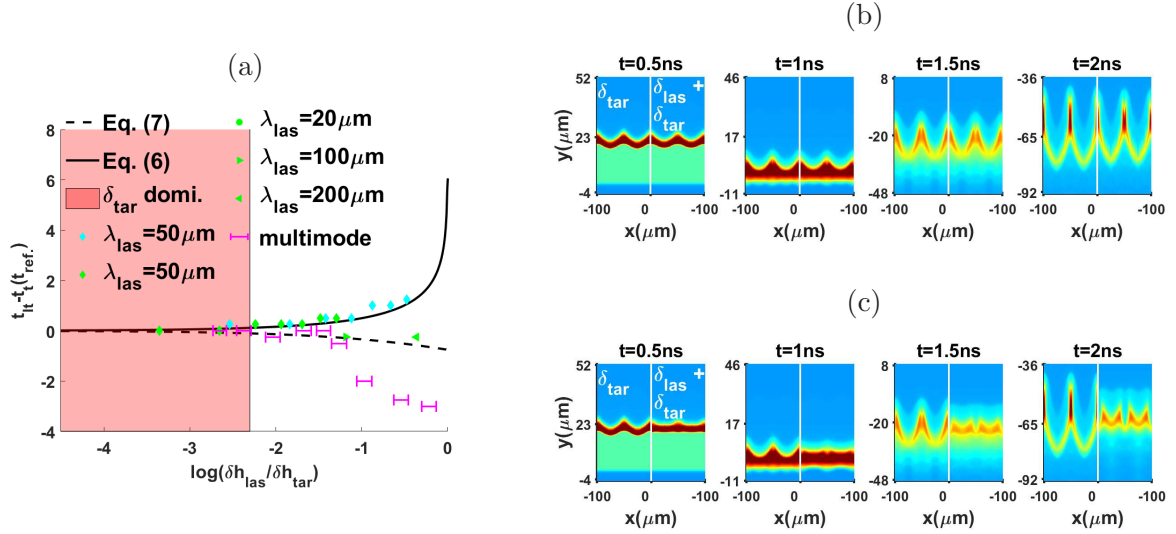


FIG. 4: (a) Evolution of $t_{\text{lt}} - t_t$ versus $\frac{\delta h_{\text{las}}}{\delta h_{\text{tar}}}$, plotted on a logarithmic scale and showing the same data as Fig. 2(a). (b) and (c) present simulated density profiles at $\frac{\delta h_{\text{las}}}{\delta h_{\text{tar}}} = 0.08$ (right) and $\frac{\delta h_{\text{las}}}{\delta h_{\text{tar}}} = 0.62$ (right), respectively. Inside the target-dominant regime, dominated by the red shaded region in (a), laser imprinting has little influence compared with that of only δ_{tar} , as evidenced by the similar density distribution in (b). Outside this region, however, laser imprinting strongly affects the perturbation evolution, leading to a clear differences visible in (c). Blue and green colors represent $\delta h_{\text{tar}} = 2 \mu\text{m}$ and $\delta h_{\text{tar}} = 4 \mu\text{m}$, respectively. For each subplot in (b) and (c), the left panel corresponds to simulations including only δ_{tar} , while the right panel corresponds to simulations including both δ_{las} and δ_{tar} . Each subplot has an equal size and the color bar follows that of Fig. 3(a).

Fig. 4 validates Eq. (6) and Eq. (7) through cases 17-42. The simulation parameters are listed in Table III in the Appendix. Within the target-dominant region, diamonds of various colors align closely with Eq. (6), as the in-phase δ_{las} and δ_{tar} share a wavelength of $50 \mu\text{m}$. Simulations were also performed for cases where the single-mode δ_{las} and δ_{tar} possess different wavelengths (denoted by circles and triangles), in agreement with Eq. (7). The agreement indicates that when δ_{las} and δ_{tar} become out of phase, their combined effect can be interpreted as that of antiphased perturbations. This is justified because the onset of the nonlinear stage is determined by the maximum perturbation amplitude. Magenta symbols, which represent multimode, provide further

support for Eq. (7), which overlaps with Eq. (9). Here, the simulated nonlinear onset time is defined as when the maximum deformation reaches $0.1\lambda_{\max}$, where λ_{\max} denotes the maximum target perturbation wavelength. The intensity range of the laser imprinting is closely related with the wavelength range of laser perturbations. Broader spectral widths produce larger horizontal error bars. Notably, when perturbations have already entered the nonlinear stage by the onset of acceleration, the advanced nonlinear onset time is not included in the model. This explains why three error bars deviate significantly from Eq. (7).

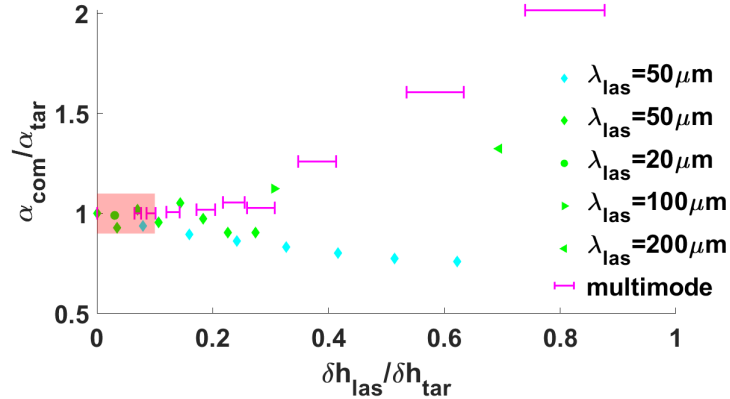


FIG. 5: Mass weighted adiabat $\frac{\alpha_{\text{com}}}{\alpha_{\text{tar}}} \sim \left(\frac{P_{\text{com}} \rho_{\text{tar}}^3}{P_{\text{tar}} \rho_{\text{com}}^3} \right)_{\text{mass}}$ versus $\frac{\delta h_{\text{las}}}{\delta h_{\text{tar}}}$. Symbols follow the same convention as Fig. 4. Within the target-dominant region (red shaded), laser imprinting alters the adiabat by less than 12% relative to the case with only δ_{tar} .

We also evaluate the effect of laser imprinting on the target's mass-weighted adiabat, expressed as

$$\frac{\alpha_{\text{com}}}{\alpha_{\text{tar}}} \sim \left(\frac{P_{\text{com}} \rho_{\text{tar}}^3}{P_{\text{tar}} \rho_{\text{com}}^3} \right)_{\text{mass}},$$

where α_{com} , P_{com} and ρ_{com} denote the adiabat, pressure, and density for simulations with both perturbations, and α_{tar} , P_{tar} and ρ_{tar} refer to simulations with only target perturbations. As shown in Fig. 5, within the target-dominant region, the deviation in adiabat remains below 12% relative to simulations with only δ_{tar} . Combining the results shown in Fig. 4 and Fig. 5, we conclude that the imprinting sensitivity threshold defined by $\delta h_{\text{las}}/\delta h_{\text{tar}} = 0.1$ effectively ensures that the influence of laser imprinting on both the nonlinear onset time and the adiabat remains little.

C. Experimental validation for imprinting sensitivity

The imprinting sensitivity is supported by OMEGA implosion experiments [39]. These experiments were designed to systematically probe the dependence of implosion performance on the level of laser imprinting.

On kilojoule-scale cryogenic DT targets, the imprinting level was modulated by varying the SSD bandwidth. The resulting on-target laser nonuniformity σ_{las} is related to the SSD fraction by

$$\sigma_{\text{las}} \approx \frac{20\%}{\sqrt{47.5 \times \text{SSD}_{\text{fraction}} + 1}}, \quad (10)$$

where $\text{SSD}_{\text{fraction}}$ ranges from 15% to 100%. Laser imprinting modes with $l > 20$ dominate the total nonuniformity. The experimental results show that for the high-adiabat design ($\alpha \approx 5$), the neutron yield becomes insensitive to imprinting once σ_{las} falls below approximately 4%. Here σ_{las} represents the total on-target illumination nonuniformity calculated using hard sphere (no plasma) superposition of 60 beam profiles. This threshold is notably lower than the previously reported 1% [35]. High-dimensional simulations attribute this difference to the combined effects of target perturbations and plasma smoothing.

σ_{las}	3%	4%	5%	6%	7%	8%
$\sigma_{\text{tar}}(\mu\text{m})$	0.4	0.4	0.4	0.4	0.4	0.4
S_{omega}	N	N	Y	Y	Y	Y
$\frac{\delta h_{\text{las}}}{\delta h_{\text{tar}}}$	0.08	0.1	0.13	0.15	0.18	0.20

TABLE I: Sensitivity of OMEGA implosion experiments to laser imprinting S_{omega} , where "N" denotes insensitive and "Y" denotes sensitive. The total on-target illumination nonuniformity σ_{las} was calculated using hard sphere (no plasma) superposition of 60 beam profiles, yielding $\sigma_{\text{las}} \approx 20.3(\%)/\sqrt{47.5 \times \text{SSD}_{\text{fraction}} + 1}$. The amplitude of target perturbations σ_{tar} corresponds to a $\pm 0.4 \mu\text{m}$ variation in the CD ablator thickness.

Our quantitative laser imprinting sensitivity incorporates both target perturbations and plasma smoothing. Stronger plasma smoothing reduces imprinting efficiency, and this reduction, when combined with larger target perturbations, decreases the overall implosion sensitivity to laser nonuniformity. To apply this sensitivity, we performed 1D MULTI simulations [43] using the experimental pulse shape and target design to calculate the time-dependent ablative velocity and

conduction zone under non-steady conditions. For the dominant imprinting mode ($l = 20$), the perturbation in ablative velocity was derived from Eq. 3 with $\frac{\delta I_L}{I_L} = \sigma_{\text{las}}$, and the corresponding imprinting amplitude δh_{las} was obtained via Eq. 4. The results, summarized in Table I, show that OMEGA implosion performance remained insensitive to laser imprinting when $\delta h_{\text{las}}/\delta h_{\text{tar}} \leq 0.10$. Hence, $\delta h_{\text{las}}/\delta h_{\text{tar}}$, which inherently includes the effects of target imperfections and plasma smoothing, provides a practical metric to assess imprinting sensitivity.

The sensitivity threshold of implosion performance to target surface defects can also be derived from the model derivation section, yielding $\delta h_{\text{tar}}/\delta h_{\text{las}} = 0.10$. This result indicates that for OMEGA implosions using 100%-bandwidth SSD, the rms of target perturbations need to be reduced to $3 \times 10^{-3} \pm \mu\text{m}$ such that implosion performance becomes dominated by laser imprinting. This requirement exceeds the current capability of target fabrication, making target quality a critical determinant of current implosion performance.

D. Implication for joint control of laser and target perturbations

The quantified sensitivity to laser imprinting, formulated as Eq. 8, suggests a practical strategy to jointly control laser (δh_{las}) and target (δh_{tar}) perturbations. When $\delta h_{\text{las}}/\delta h_{\text{tar}} \geq 0.1$, implosion performance can be enhanced more effectively by improving laser uniformity. Conversely, when $\delta h_{\text{las}}/\delta h_{\text{tar}} < 0.1$, greater performance can be achieved by improving target fabrication.

To demonstrate this strategy, multimode perturbation simulations were performed. The temporal evolution of the shell density under different imprinting ratios is shown in Fig. 6. Fig. 6(b) shows that a higher imprinting ratio ($\delta h_{\text{las}}/\delta h_{\text{tar}} \approx 0.22\text{-}0.26$) leads to substantial shell deformation and the development of secondary asymmetries, notably in the highlighted areas, which further degrades implosion performance. In contrast, for a low imprinting ratio ($\frac{\delta h_{\text{las}}}{\delta h_{\text{tar}}} \approx 0.07\text{-}0.08$), the shell structure is virtually indistinguishable from the case with no laser imprinting. This confirms that laser imprinting has a negligible impact on performance degradation when $\frac{\delta h_{\text{las}}}{\delta h_{\text{tar}}} \leq 0.1$.

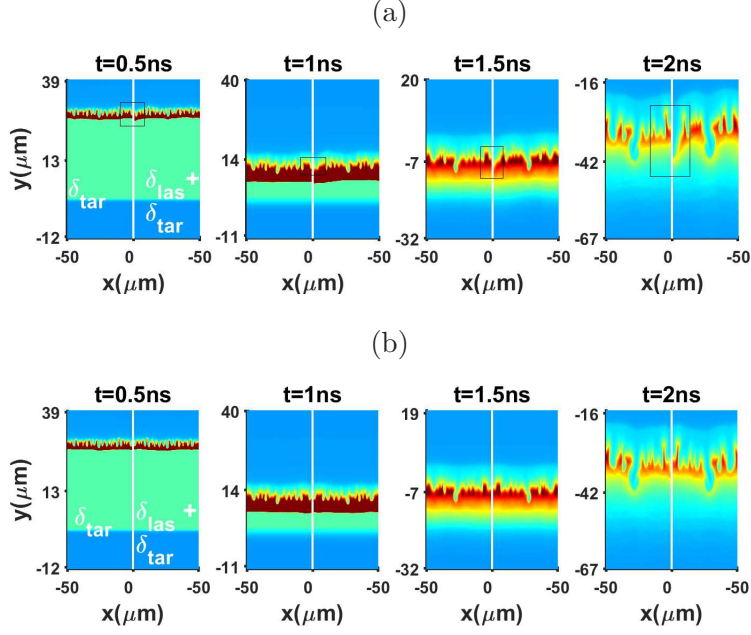


FIG. 6: Temporal evolution of density under different levels of laser imprinting for multimode perturbations. In (a), the right panel in each subplot has a higher $\frac{\delta h_{\text{las}}}{\delta h_{\text{tar}}} = 0.22 \sim 0.26$ and shows clear degradation in shell integrity, especially in the boxed area. In (b), the right panel in each subplot corresponds to a low imprinting ratio of $\frac{\delta h_{\text{las}}}{\delta h_{\text{tar}}} = 0.07 \sim 0.08$, where the shell integrity is similar to the left, $\frac{\delta h_{\text{las}}}{\delta h_{\text{tar}}} = 0$. Each subplot has an equal size and the color bar follows that of Fig. 3(a).

IV. CONCLUSIONS

In conclusion, this study develops an equivalent perturbation model for direct-drive ICF that quantifies laser imprinting as target surface imperfections. The model identifies a implosion sensitivity to laser imprinting $\frac{\delta h_{\text{las}}}{\delta h_{\text{tar}}} = 0.1$. When $\frac{\delta h_{\text{las}}}{\delta h_{\text{tar}}} \leq 0.1$, laser imprinting alters the nonlinear onset time and adiabat at the start of acceleration by less than 12%, compared to simulations with target perturbations alone. Moreover, the implosion sensitivity to laser imprinting is supported by OMEGA experiments. These results indicate that joint control of laser and target perturbations, improving target quality when $\frac{\delta h_{\text{tar}}}{\delta h_{\text{las}}} \leq 0.1$ and laser smoothing otherwise, can support stable implosions for high-gain direct-drive inertial confinement fusion. The current equivalent perturbation model is based on steady ablation theory and has been extended to unsteady ablation under complex pulse designs. Future work will extend the model to more internal target perturbations.

Acknowledgments

This work is supported by National Natural Science Foundation of China (Grant No. 12375242), and Science Challenge Project (Grant No. TZ2025014).

Data Availability Statement

Data available on request from the authors.

V. APPENDIX

Table II lists simulation cases that satisfy $\frac{\delta h_{\text{las}}}{\delta h_{\text{tar}}} \approx 1$ when $D_{ac} \approx 1$. These cases were simulated using the two-dimensional Eulerian radiation-hydrodynamic code FLASH [42] to validate Eq. (4). A common setup was used for all simulations. A planar CH target with a density of 1 g/cm^3 is placed at $Y = [0 \text{ } \mu\text{m}, 40 \text{ } \mu\text{m}]$. The vertically incident laser employs third-harmonic and offers two types of pulse shapes. Pulse-A is a square pulse with a rise time of 0.1 ns and a peak intensity of 100 TW/cm^2 . Pulse-B is also a square pulse with a longer rise time of 0.5 ns and a peak intensity of 75 TW/cm^2 . Compared to Pulse-A, Pulse-B is designed to enhance the imprinting of laser perturbations. The simulation domain has dimensions of $L_X = (1 - 4)\lambda$ in the X-direction and $L_Y = [-400 \text{ } \mu\text{m}, 200 \text{ } \mu\text{m}]$ in the Y-direction, with a spatial resolution ranging from $0.13 \text{ } \mu\text{m}$ to $0.52 \text{ } \mu\text{m}$. Here, λ represents the single-mode perturbation wavelength applied to both the laser and the target. δ_{las} is defined as $\frac{\delta I_L}{I_L} = \mathcal{A} \cos(2\pi x/\lambda)$, and δ_{tar} is defined as $\delta h_{\text{tar}} = \delta h \cos(2\pi x/\lambda)$, where the amplitude δh is either $2 \text{ } \mu\text{m}$ or $4 \text{ } \mu\text{m}$.

pulse case	$\frac{\delta I_L}{I_L}$	$t_{\text{load}}(\text{ns})$	$\lambda(\mu\text{m})$	$\delta h_{\text{tar}}(\mu\text{m})$	pulse case	$\frac{\delta I_L}{I_L}$	$t_{\text{load}}(\text{ns})$	$\lambda(\mu\text{m})$	$\delta h_{\text{tar}}(\mu\text{m})$		
A	1	0.96	0.2	30	/	A	5	/	/	30	2
A	2	0.7	0.3	50	/	A	6	/	/	50	2
A	3	0.64	0.5	100	/	A	7	/	/	100	4
A	4	0.38	0.9	150	/	A	8	/	/	150	4
B	9	0.62	0.3	30	/	B	13	/	/	30	2
B	10	0.36	0.5	50	/	B	14	/	/	50	2
B	11	0.55	0.6	70	/	B	15	/	/	70	4
B	12	0.38	0.9	100	/	B	16	/	/	100	4

TABLE II: Information of simulation cases with one kind of perturbation. Here, t_{load} represents the imprinting time of laser perturbations, and it increases with λ .

The cases in Table III feature both δ_{las} and δ_{tar} . These cases were simulated to investigate the influence of laser imprinting on the onset time of the nonlinear stage and on the adiabat, compared to cases with only δ_{tar} . The common simulation setup is identical to that described for Table II. The multimode δ_{las} is prescribed as: $\frac{\delta I_L}{I_L} = \mathcal{A}(\cos(2\pi x/30 + \phi_1) + \cos(2\pi x/40 + \phi_2) + \cos(2\pi x/60 + \phi_3) + \cos(2\pi x/100 + \phi_4))$, where x is in unit of μm . The multimode δ_{tar} is set as $\delta h_{\text{tar}} = 100k^{-2} \sum \cos(2\pi/200 * nx + \phi)(\mu\text{m})$, where n is an integer ranging from 4 to 10, ϕ and ϕ_{1-4} are random phase uniformly distributed between zero and one.

pulse case	$\frac{\delta I_L}{I_L}$	t_{load} (ns)	$\lambda_{\text{tar}}(\mu\text{m})$ $/\lambda_{\text{las}}(\mu\text{m})$	δh_{tar} (μm)		pulse case	$\frac{\delta I_L}{I_L}$	t_{load} (ns)	$\lambda_{\text{tar}}(\mu\text{m})$ $/\lambda_{\text{las}}(\mu\text{m})$	δh_{tar} (μm)	
A	17	0.0	0.3	50/50	4	A	30	0.3	0.3	50/50	2
A	18	0.1	0.3	50/50	4	A	31	0.4	0.3	50/50	2
A	19	0.2	0.3	50/50	4	A	32	0.5	0.3	50/50	2
A	20	0.3	0.3	50/50	4	A	33	0.6	0.3	50/50	2
A	21	0.4	0.3	50/50	4	A	34	0.7	0.3	50/50	2
A	22	0.5	0.3	50/50	4	B	35	0.0	0.9	multimode	2
A	23	0.6	0.3	50/50	4	B	36	0.05	0.9	multimode	2
A	24	0.7	0.3	50/50	4	B	37	0.07	0.9	multimode	2
A	25	0.3	0.2	50/30	4	B	38	0.1	0.9	multimode	0.76
A	26	0.3	0.5	50/100	4	B	39	0.15	0.9	multimode	0.76
A	27	0.3	0.9	50/200	4	B	40	0.2	0.9	multimode	0.76
A	28	0.1	0.3	50/50	2	B	41	0.3	0.9	multimode	0.76
A	29	0.2	0.3	50/50	2	B	42	0.4	0.9	multimode	0.76

TABLE III: The information of simulation cases with both perturbations.

-
- [1] H. Abu-Shawareb, R. Acree, P. Adams, J. Adams, B. Addis, R. Aden, P. Adrian, B. B. Afeyan, M. Aggleton, L. Aghaian, et al., *Physical Review Letters* **129**, 075001 (2022).
- [2] A. Kritcher, A. Zylstra, D. Callahan, O. Hurricane, C. Weber, D. Clark, C. Young, J. Ralph, D. Casey, A. Pak, et al., *Physical Review E* **106**, 025201 (2022).
- [3] H. Abu-Shawareb, R. Acree, P. Adams, J. Adams, B. Addis, R. Aden, P. Adrian, B. B. Afeyan, M. Aggleton, L. Aghaian, et al., *Physical Review Letters* **132**, 065102 (2024).
- [4] R. S. Craxton, K. S. Anderson, T. R. Boehly, V. Goncharov, D. Harding, J. Knauer, R. McCrory, P. McKenty, D. Meyerhofer, J. Myatt, et al., *Physics of Plasmas* **22**, 110501 (2015).
- [5] S. E. Bodner, *Physical Review Letters* **33**, 761 (1974).
- [6] V. A. Smalyuk, O. Sadot, J. A. Delettrez, D. D. Meyerhofer, S. P. Regan, and T. C. Sangster, *Physical Review Letters* **95**, 215001 (2005).

- [7] V. N. Goncharov, O. V. Gotchev, E. Vianello, T. R. Boehly, J. P. Knauer, P. W. McKenty, P. B. Radha, S. P. Regan, T. C. Sangster, S. Skupsky, et al., *Physics of plasmas* **13**, 012702 (2006).
- [8] D. X. Liu, T. Tao, J. Li, Q. Jia, and J. Zheng, *Physics of Plasmas* **29**, 072707 (2022).
- [9] A. Pak, Tech. Rep., Lawrence Livermore National Laboratory (LLNL), Livermore, CA (United States) (2023).
- [10] Y. Zhou, J. D. Sadler, and O. A. Hurricane, *Annual Review of Fluid Mechanics* **57**, 197 (2025).
- [11] Z. Lin, H. Luo, G. Zhu, H. Cai, S. Zhu, and M. Luo, *Nuclear Fusion* **66**, 026023 (2026).
- [12] D. Michel, S. Hu, A. Davis, V. Y. Glebov, V. Goncharov, I. Igumenshchev, P. Radha, C. Stoeckl, and D. Froula, *Physical Review E* **95**, 051202 (2017).
- [13] H. Takabe, K. Mima, L. Montierth, and R. Morse, *The Physics of fluids* **28**, 3676 (1985).
- [14] V. N. Goncharov, R. Betti, R. L. McCrory, and C. P. Verdon, *Physics of Plasmas* **3**, 4665 (1996).
- [15] R. Betti, V. N. Goncharov, R. McCrory, P. Sorotokin, and C. P. Verdon, *Physics of Plasmas* **3**, 2122 (1996).
- [16] V. N. Goncharov, *Physical Review Letters* **88**, 134502 (2002).
- [17] O. Sadot, V. A. Smalyuk, J. A. Delettrez, D. D. Meyerhofer, T. C. Sangster, R. Betti, V. N. Goncharov, and D. Shvarts, *Physical Review Letters* **95**, 265001 (2005).
- [18] H. Zhang, R. Betti, R. Yan, D. Zhao, D. Shvarts, and H. Aluie, *Physical Review Letters* **121**, 185002 (2018).
- [19] H. Zhang, R. Betti, R. Yan, and H. Aluie, *Physics of Plasmas* **27**, 122701 (2020).
- [20] T. Dittrich, O. Hurricane, D. Callahan, E. Dewald, T. Döppner, D. Hinkel, L. Berzak Hopkins, S. Le Pape, T. Ma, J. Milovich, et al., *Physical review letters* **112**, 055002 (2014).
- [21] T. Tao, G. Zheng, Q. Jia, R. Yan, and J. Zheng, *High Power Laser Science and Engineering* **11**, e41 (2023).
- [22] S. Fujioka, A. Sunahara, K. Nishihara, N. Ohnishi, T. Johzaki, H. Shiraga, K. Shigemori, M. Nakai, T. Ikegawa, M. Murakami, et al., *Physical review letters* **92**, 195001 (2004).
- [23] G. Zheng, T. Tao, Q. Jia, R. Yan, and J. Zheng, *Plasma Physics and Controlled Fusion* **64**, 105003 (2022).
- [24] S. Hu, W. Theobald, P. Radha, J. Peebles, S. Regan, A. Nikroo, M. Bonino, D. Harding, V. Goncharov, N. Petta, et al., *Physics of Plasmas* **25** (2018).

- [25] Z. Li, X. Yang, G. Zhang, B. Zeng, B. Xu, Z. Chen, Y. Ma, F. Shao, and J. Zhang, *Nuclear Fusion* **65**, 066024 (2025).
- [26] I. Igumenshchev, V. Goncharov, F. Marshall, J. Knauer, E. Campbell, C. Forrest, D. Froula, V. Y. Glebov, R. McCrory, S. Regan, et al., *Physics of Plasmas* **23** (2016).
- [27] S. Miller and V. N. Goncharov, *Physics of Plasmas* **29** (2022).
- [28] Z. Lei, J. Li, L. Wang, Z. Chen, J. Li, S. Zou, J. Wu, Y. Liu, Z. Yan, G. Yang, et al., *Plasma Physics and Controlled Fusion* **66**, 125015 (2024).
- [29] Y. Liu, Z. Li, Z. Yan, J. Dong, Z. Fang, Z. Chen, J. Li, J. Wu, W. Wang, L. Wang, et al., *Nuclear Fusion* **66**, 016019 (2025).
- [30] M. Pokornik, S. Khan, J. Gaffney, B. MacGowan, A. Maris, K. Humbird, and S. Haan, *Nuclear Fusion* **65**, 076016 (2025).
- [31] K. O. Mikaelian, *Physics of Fluids* **17** (2005).
- [32] Y. Aglitskiy, A. Velikovich, M. Karasik, N. Metzler, S. Zalesak, A. Schmitt, L. Phillips, J. Gardner, V. Serlin, J. Weaver, et al., *Philosophical Transactions of the Royal Society A: Mathematical, Physical and Engineering Sciences* **368**, 1739 (2010).
- [33] Y. Kato and K. Mima, *Appl. Phys. B* **29**, 186 (1982).
- [34] Y. Kato, K. Mima, N. Miyanaga, S. Arinaga, Y. Kitagawa, M. Nakatsuka, and A. Yamanaka, *Physical Review Letters* **53**, 1057 (1984).
- [35] S. Skupsky and K. Lee, *Journal of Applied Physics* **54**, 3662 (1983).
- [36] S. Skupsky, R. Short, T. Kessler, R. Craxton, S. Letzring, and J. Soures, *Journal of Applied Physics* **66**, 3456 (1989).
- [37] T. Boehly, V. Smalyuk, D. Meyerhofer, J. Knauer, D. Bradley, R. Craxton, M. Guardalben, S. Skupsky, and T. Kessler, *Journal of applied physics* **85** (1999).
- [38] K. Tsubakimoto, M. Nakatsuka, H. Nakano, T. Kanabe, T. Jitsuno, and S. Nakai, *Optics communications* **91**, 9 (1992).
- [39] D. Patel, J. Knauer, D. Cao, R. Betti, R. Nora, A. Shvydky, V. Gopaldaswamy, A. Lees, S. Sampat, W. Donaldson, et al., *Physical Review Letters* **131**, 105101 (2023).
- [40] F. Dahmani and T. Kerdja, *Physical Review A* **44**, 2649 (1991).
- [41] S. W. Haan, *Physical Review A* **39**, 5812 (1989).
- [42] B. Fryxell, K. Olson, P. Ricker, F. X. Timmes, M. Zingale, D. Q. Lamb, P. MacNeice, R. Rosner, J. W. Truran, and H. Tufo, *The Astrophysical Journal Supplement Series* **131**, 273 (2000).

- [43] R. Ramis, R. Schmalz, and J. Meyer-ter Vehn, *Computer Physics Communications* **49**, 475 (1988).